Structural Chromosomal Rearrangements Require Nucleotide-Level Resolution: Lessons from Next-Generation Sequencing in Prenatal Diagnosis

Zehra Ordulu,[1,2] Tammy Kammin,[1] Harrison Brand,[3,4,5] Vamsee Pillalamarri,[3] Claire E. Redin,[2,3,4,5] Ryan L. Collins,[3] Ian Blumenthal,[3] Carrie Hanscom,[3] Shahrin Pereira,[1] India Bradley,[6] Barbara F. Crandall,[6] Pamela Gerrol,[1] Mark A. Hayden,[1] Naveed Hussain,[7] Bibi Kanengisser-Pines,[8] Sibel Kantarci,[9] Brynn Levy,[10] Michael J. Macera,[11] Fabiola Quintero-Rivera,[9] Erica Spiegel,[12] Blair Stevens,[13] Janet E. Ulm,[14] Dorothy Warburton,[15,16] Louise E. Wilkins-Haug,[1,2] Naomi Yachelevich,[17] James F. Gusella,[3,4,5,18] Michael E. Talkowski,[2,3,4,5,19] and Cynthia C. Morton[1,2,5,20,21,*]

In this exciting era of "next-gen cytogenetics," integrating genomic sequencing into the prenatal diagnostic setting is possible within an actionable time frame and can provide precise delineation of balanced chromosomal rearrangements at the nucleotide level. Given the increased risk of congenital abnormalities in newborns with de novo balanced chromosomal rearrangements, comprehensive interpretation of breakpoints could substantially improve prediction of phenotypic outcomes and support perinatal medical care. Herein, we present and evaluate sequencing results of balanced chromosomal rearrangements in ten prenatal subjects with respect to the location of regulatory chromatin domains (topologically associated domains [TADs]). The genomic material from all subjects was interpreted to be "normal" by microarray analyses, and their rearrangements would not have been detected by cell-free DNA (cfDNA) screening. The findings of our systematic approach correlate with phenotypes of both pregnancies with untoward outcomes (5/10) and with healthy newborns (3/10). Two pregnancies, one with a chromosomal aberration predicted to be of unknown clinical significance and another one predicted to be likely benign, were terminated prior to phenotype-genotype correlation (2/10). We demonstrate that the clinical interpretation of structural rearrangements should not be limited to interruption, deletion, or duplication of specific genes and should also incorporate regulatory domains of the human genome with critical ramifications for the control of gene expression. As detailed in this study, our molecular approach to both detecting and interpreting the breakpoints of structural rearrangements yields unparalleled information in comparison to other commonly used first-tier diagnostic methods, such as non-invasive cfDNA screening and microarray analysis, to provide improved genetic counseling for phenotypic outcome in the prenatal setting.

Introduction

Fetal material obtained through invasive methods can be assessed routinely with different techniques, including karyotyping, fluorescence in situ hybridization, and chromosomal microarray analysis (CMA).[1–3] Although karyotyping remains the principal cytogenetic tool in prenatal diagnosis, CMA has the advantage of higher resolution and is the preferred method in a fetus with one or more major structural abnormalities identified by ultrasonography.[1] However, unlike karyotyping, CMA cannot detect balanced chromosomal rearrangements, such as translocations, inversions, and insertions.

The risk of congenital abnormalities is two to three times higher in newborns with apparently balanced de novo chromosomal rearrangements (6.1% for translocations and 9.4% for inversions) than in a population of pregnancies tested by amniocentesis.[4] The cause of the increase in abnormal phenotypes in such cases can be a submicroscopic deletion, duplication, disruption, dysregulation, or fusion of a gene(s) located at or near the breakpoints. Studies using CMA have demonstrated the presence of a cryptic imbalance in 40%–50% of subjects with an abnormal

[1]Department of Obstetrics, Gynecology, and Reproductive Biology, Brigham and Women's Hospital, Boston, MA 02115, USA; [2]Harvard Medical School, Boston, MA 02115, USA; [3]Center for Human Genetic Research, Massachusetts General Hospital, Boston, MA 02114, USA; [4]Department of Neurology, Massachusetts General Hospital and Harvard Medical School, Boston, MA 02114, USA; [5]Program in Medical and Population Genetics, Broad Institute of MIT and Harvard, Boston, MA 02142, USA; [6]Department of Psychiatry, Prenatal Diagnosis Center, David Geffen School of Medicine, University of California, Los Angeles, Medical Plaza, Los Angeles, CA 90095, USA; [7]Department of Pediatrics, Connecticut Children's Medical Center, University of Connecticut, Farmington, CT 06030, USA; [8]Department of Obstetrics and Gynecology, Kaplan Medical Center, Rehovot 76100, Israel; [9]Department of Pathology and Laboratory Medicine, UCLA Clinical Genomics Center, David Geffen School of Medicine, University of California, Los Angeles, Los Angeles, CA 90095, USA; [10]Department of Pathology and Cell Biology, College of Physicians and Surgeons, Columbia University, New York, NY 10032, USA; [11]New York Presbyterian Hospital, Columbia University Medical Center, New York, NY 10032, USA; [12]Department of Maternal Fetal Medicine, Columbia University Medical Center, New York, NY 10032, USA; [13]Department of Obstetrics, Gynecology, and Reproductive Sciences, University of Texas Medical School at Houston, Houston, TX 77030, USA; [14]Regional Obstetrical Consultants, Chattanooga, TN 37403, USA; [15]Department of Genetics and Development, Columbia University, New York, NY 10032, USA; [16]Department of Pediatrics, Columbia University, New York, NY 10032, USA; [17]Department of Pediatrics, Clinical Genetics Services, New York University School of Medicine, New York, NY 10003, USA; [18]Department of Genetics, Harvard Medical School, Boson, MA 02115, USA; [19]Departments of Psychiatry and Pathology, Massachusetts General Hospital, Boston, MA 02114, USA; [20]Department of Pathology, Brigham and Women's Hospital and Harvard Medical School, Boston, MA 02115, USA; [21]Division of Evolution and Genomic Science, School of Biological Sciences, University of Manchester, Manchester Academic Health Science Center, Manchester 03101, UK

*Correspondence: cmorton@partners.org

http://dx.doi.org/10.1016/j.ajhg.2016.08.022.

Table 1. Pathological Rewiring of Genetic Regulatory Interactions

Genomic Locus on 2q36.1	TAD and TBR Nucleotides (hESC, GRCh37/hg19)[18] (Size)	Structural Rearrangement (Associated Phenotype)
WNT6-IHH-DES	TBR: 219,731,756–219,851,756 (120 kb), TAD: 219,851,756–220,251,756 (400 kb), TBR: 220,251,756–220,411,756 (160 kb)	inversion or duplication altering the 160 kb TBR and bringing the centromeric portion of the *EPHA4*-containing TAD into proximity with *WNT6* (F-syndrome [MIM: 102510])
		duplication or deletion altering the 160 kb TBR and bringing *IHH* into proximity with the centromeric portion of the *EPHA4*-containing TAD (polydactyly)
EPHA4	TAD: 220,411,756–222,891,756 (2.48 Mb)	deletion involving the TBR at 222,891,756 (brachydactyly)
PAX3	TAD: 222,891,756–223,491,756 (600 kb)	

This table shows the pathological rewiring of genetic regulatory interactions of enhancer *EPHA4* through different structural rearrangements altering the TAD boundaries (data presented herein are modified from Lupiãnez et al.[20]). Abbreviations are as follows: hESC, human embryonic stem cell; TAD, topologically associated domain; and TBR, topological boundary region.

phenotype and an apparently balanced chromosomal rearrangement.[5–12] Massively parallel sequencing technologies can provide timely localization of chromosomal breakpoints with nucleotide-level precision in all apparently balanced rearrangements, along with information on the gain or loss of genomic material,[13,14] which could substantially improve the prediction of phenotypic outcomes and support perinatal medical care.

Outcomes of structural rearrangements changing the copy number of a gene or directly disrupting a gene can be predicted from dosage effects. However, if a balanced rearrangement occurs in a non-coding region or the regulatory effect of the rearrangement is more pertinent to an abnormal phenotype than the directly affected gene, predicting pathogenic consequences can become challenging and even erroneous when only the gene(s) with copy-number changes or disrupted gene(s) are evaluated. This is particularly important in prenatal diagnosis, because for many key developmental genes, *cis*-regulatory elements can extend beyond the transcription unit with an estimated median regulator-target gene distance of 120 kb,[15] which can range up to 1.5 Mb.[16,17]

Topologically associated domains (TADs) have been elucidated as key elements of mammalian regulatory organization.[18,19] TADs are highly conserved megabase-sized genomic segments that partition the genome into large units with frequent intra-domain interactions. They are separated by topological boundary regions (TBRs), which represent "genomic insulators" by blocking the interactions between adjacent TADs. Disruption of TBRs by structural rearrangements has been demonstrated to cause rewiring of genomic regulators in the *WNT6-IHH-EPHA4-PAX3* locus (MIM: 604663, 600726, 602188, and 606597) and result in human limb malformations, as described by Lupiãnez et al. (Table 1 and Figure 1).[20] In this context, the developmental genes with historically well-known long-range regulation can be re-evaluated in relation to their TAD and TBR annotations (Table 2 and Figure 1). For example, disruption of *PAX6* (MIM: 607108) and regulatory elements located in the same TAD as *PAX6* (up to 150 kb downstream) results in isolated aniridia,[21] whereas haploinsufficiency of *WT1* (MIM: 194070), which is located in the TAD adjacent to *PAX6*, causes genitourinary anomalies without aniridia.[23] Deletions of the contiguous locus containing both *PAX6* and *WT1*, including the TBR between their two adjacent TADs, result in the autosomal-dominant WAGR syndrome (MIM: 194072) with both aniridia and genitourinary anomalies, supporting the "genomic insulator" role of TBRs. In addition, the size of an individual TAD can be relevant to the extent of long-range regulation. *TWIST1* (MIM: 601622) is known to have long-range regulation up to 260 kb downstream, which is located within the same 440 kb TAD as *TWIST1*. Monoallelic disruption of both *TWIST1* and its downstream regulatory region results in Saethre-Chotzen syndrome (MIM: 101400).[24] *SOX9* (MIM: 608160) is reported to have long-range regulation up to 1.5 Mb upstream, which is located within the same 1.88 Mb TAD as *SOX9*. Monoallelic disruption of both *SOX9* and its regulatory region is associated with campomelic dysplasia (MIM: 114290) and Pierre Robin sequence (MIM: 261800).[25,28,29] There might also be phenotype-specific regulators within the same TAD for a developmental gene depending on their distance from the gene of interest. Monoallelic disruption of regulatory elements located within the same 1.6 Mb TAD as *SHH* (MIM: 600725) can result in type 3 holoprosencephaly (MIM: 142945) or preaxial polydactyly (MIM: 174500), depending on the location (265 kb upstream or 1 Mb upstream of *SHH*, respectively).[26] Lastly, in addition to the genes showing a phenotype with monoallelic disruption, regulatory regions of developmental genes located on the X chromosome or imprinted genes should also be carefully analyzed, given that disruption of a single allele through balanced rearrangements could result in an abnormal phenotype in such cases. For instance, *POU3F4* (MIM: 300039) is an X-linked recessively inherited gene with long-range regulation up to 900 kb upstream[27] in a 3.04 Mb TAD, and disruption of a single allele of *POU3F4* or its regulatory region results in deafness in males. Overall, advances in the understanding of chromatin organization of the human genome, along with

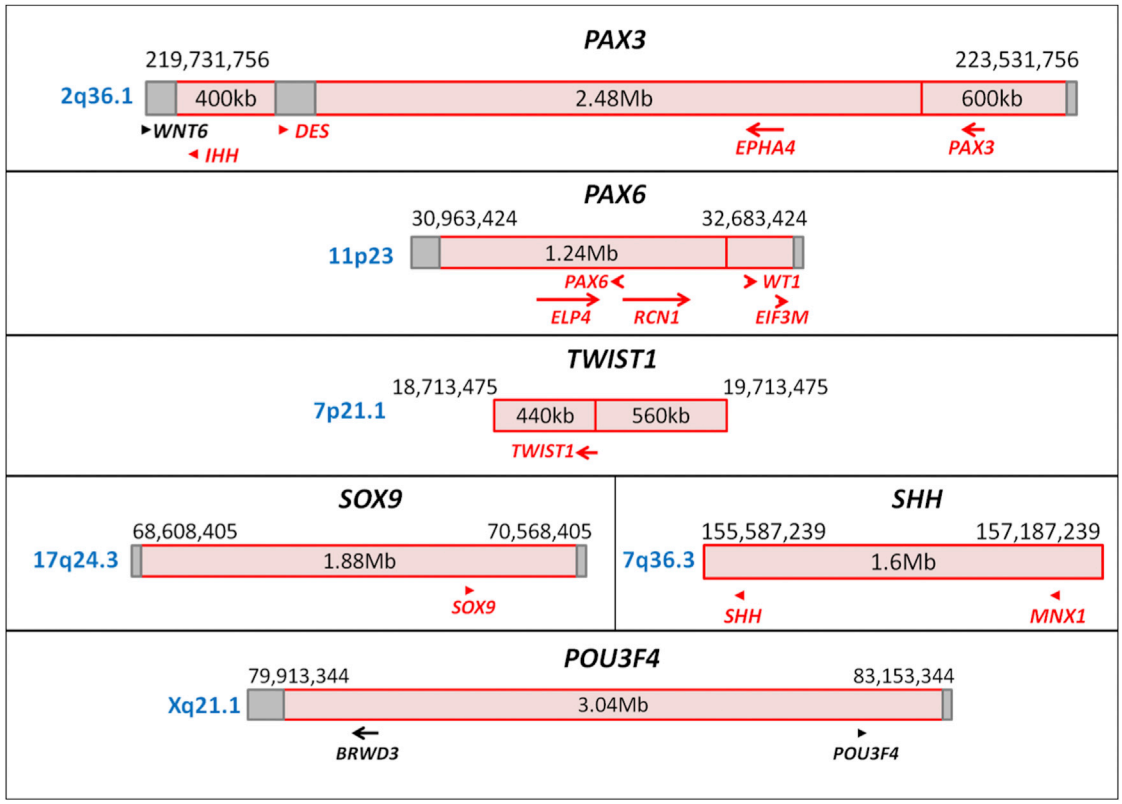

Figure 1. Developmental Genes with Well-Known Long-Range Regulations
Schematic diagrams of representative developmental genes with well-known long-range regulations in relation to their TAD (red box) and TBR (dark-red vertical line if 0 bp or gray box if greater than 0 bp) annotations (genes in red: haploinsufficiency index < 10%).

the evolving databases of phenotypes associated with structural variation, could provide a conceptual framework for the interpretation of balanced-rearrangement breakpoints and their potential *cis*-regulatory effects.

Identifying breakpoints of balanced chromosomal rearrangements has been the foundation of the Developmental Genome Anatomy Project (DGAP), which has sequenced more than 200 subjects. As an extension of these efforts, in this study, we sequenced ten prenatal subjects with balanced chromosomal rearrangements by using customized large-insert libraries and used publicly available databases to interpret the breakpoints on the basis of convergent genomic evidence in light of previously annotated TADs and TBRs in human embryonic stem cells.[29]

Material and Methods

Subjects

Ten subjects were enrolled after proper informed consent was acquired in accordance with an institutional-review-board protocol approved by Partners HealthCare System in Boston. These ten subjects represent the total of a consecutive series of DGAP prenatal referrals to date, and prior to enrollment, all had balanced chromosomal rearrangements according to karyotyping with normal CMA results. Two subjects (DGAP239 and DGAP259) have been reported in part previously.[30,31]

Sequencing and Bioinformatic Analysis

Genomic DNA was extracted from amniocytes or chorionic villi with a Gentra Puregene Cell Kit (QIAGEN). Large-insert structural-variation sequencing was performed as previously described.[12,26] In brief, after the production of large-insert libraries (target size of 2–3.5 kb) and quality control, massively parallel paired-end sequencing of 25 or 50 cycles was performed with an Illumina HiSeq 2000 or 2500. Reads were processed with our customized structural-variant sequencing pipelines, which include alignment, clustering of anomalous read pairs, extensive cluster filtering, and variant screening against known structural variants.[32–35] Genome-wide physical coverage of inserts ranged from 35× to 68×, and DNA input ranged from 900 ng to 5 μg. For all subjects with sufficient material, DNA was amplified by PCR with primers based on sequence reads supporting the rearrangement junction for confirmation of breakpoints.

Analysis of Convergent Genomic Evidence

In addition to genes located directly at breakpoints, phenotypic associations were evaluated in relation to previously annotated TADs and TBRs in human embryonic stem cells[18] for positional effects on protein-coding genes through disruption of potential regulatory elements. DECIPHER was utilized for predicting the probability of haploinsufficiency, which was determined on the basis of genes known to produce a phenotype through haploinsufficiency and genes disrupted by unambiguous loss-of-function variants in at least two apparently healthy individuals. Low haploinsufficiency indices (<10%) indicate a high predicted probability that a gene will exhibit haploinsufficiency (i.e., disruption

Table 2. TADs and TBRs of Genes with Historically Well-Known Long-Range *cis*-Regulation Associated with a Phenotype

Locus (Chromosome Band)	TAD and TBR Nucleotides (hESC, GRCh37/hg19)[18] (Size)	Genetic Alterations	Phenotype
PAX6-WT1 (11p23)	TBR: 30,963,424–31,083,424 (120 kb), TAD: 31,083,424–32,323,424 (1.24 Mb), TAD: 32,323,424–32,643,424 (320 kb), TBR: 32,643,424–32,683,424 (40 kb),	disruption of regulatory elements up to 150 kb downstream of *PAX6*	aniridia[21]
		deletions involving *PAX6* and *WT1*, which includes the TBR between the TADs of these genes	WAGR syndrome[22]
		haploinsufficiency of *WT1*	syndromes involving genitourinary anomalies without aniridia[23]
TWIST1 (7p21.1)	TAD: 18,713,475–19,153,475 (440 kb), TAD: 19,153,475–19,713,475 (560 kb)	disruption of regulatory elements up to 260 kb downstream of *TWIST1*	Saethre-Chotzen syndrome[24]
SOX9 (17q24.3)	TAD: 68,648,405–70,528,405 (1.88 Mb)	disruption of regulatory elements up to 1.5 Mb upstream of *SOX9*	Pierre Robin sequence[25]
SHH (7q36.3)	TAD: 155,587,239–157,187,239 (1.6 Mb)	disruption of regulatory elements up to 265 kb upstream of *SHH*	HPE3[26]
		disruption of regulatory elements up to 1 Mb upstream of *SHH*	preaxial polydactyly[26]
POU3F4 (Xq21.1)	TAD: 80,073,344–83,113,344 (3.04 Mb)	disruption of regulatory elements up to 900 kb upstream of *POU3F4*	X-linked deafness[27]

Abbreviations are as follows: hESC, human embryonic stem cell; HPE3, holoprosencephaly type 3; TAD, topologically associated domain; TBR, topological boundary region; and WAGR, Wilms tumor, aniridia, genitourinary anomalies, and mental retardation.

of one allele might be pathogenic, also referred to as monoallelic).[36] Within the analyzed intervals, disrupted genes, genes with a haploinsufficiency index < 10%, hemizygous or imprinted genes, and genes associated with a phenotype were evaluated in detail for each subject in relation to the disrupted TADs and TBRs. Abnormal phenotypic associations of disrupted or dysregulated regions were reviewed in the scientific literature, OMIM,[37] OMIM Gene Map and Morbid Map,[37] DECIPHER,[38] and the Developmental Disorders Genotype-to-Phenotype (DDG2P) database.[39]

Expression Studies

qRT-PCR was performed with RNA extracted from cultured prenatal cells of the available subjects (amniocytes from DGAP247 and chorionic villi from DGAP248 and DGAP288) and control samples (amniocytes or chorionic villi with a normal karyotype referred for advanced maternal age) or cord blood (DGAP247 and DGAP288). qRT-PCR was performed according to standard conditions of the CFX Real-Time PCR Detection System (Bio-Rad), and transcription levels were quantified with the ΔΔCT method.[30]

Results

Prior to enrollment, karyotyping was performed for all pregnancies because they were considered to be high risk (e.g., advanced maternal age, abnormal first-trimester serum screening, and/or ultrasound abnormality) with normal CMA results during clinical assessment (see Supplemental Note). Among the ten subjects analyzed, four had reciprocal translocations, five had inversions, and one had a complex rearrangement according to karyotyping. Sequencing revised the initial karyotype by providing nucleotide-level resolution to the initially described chromosome bands with a size ranging from 2.8 to 53.6 Mb, encompassing 63–1,032 genes and 16–358 phenotype-associated loci for each rearrangement (Table 3 and Table S1).[40] In addition to refining breakpoints, including those in a subject with a very complex karyotype (DGAP259), sequencing revealed cryptic rearrangements unapparent by karyotyping in four subjects (DGAP258, DGAP268, DGAP290, and DGAP295). All rearrangements were located within a TAD, except for one that was located in a TBR at Xq28 (DGAP285) (Figures 2, 3, and 4; Tables 4, 5, and 6; and Table S2). Five subjects had abnormal clinical outcomes, three continue to be healthy, and two were terminated prior to detection of any potential abnormal findings (Table 7).

DGAP239

DGAP239[30] (46,XY,t(6;8)(q13;q13)dn.arr(1-22)x2,(XY)x1.seq[GRCh37/hg19] t(6;8)(q13;q12.2)dn) had multisystemic abnormalities detected by imaging studies starting in the second trimester and was diagnosed clinically with CHARGE syndrome (MIM: 214800) only after birth. Sequencing the prenatal DNA sample identified translocation breakpoints (designated as t(6;8)(q13;q13) by karyotyping) disrupting *CHD7* (MIM: 608892) at 8q12.2 and *LMBRD1* (MIM: 612625) at 6q13 (Figure 2A and Table 4). Whereas biallelic losses of *LMBRD1* are associated with methylmalonic aciduria and homocystinuria, cblF type (MIM: 277380) (no phenotypic overlap with DGAP239),[42] monoallelic loss of *CHD7* is well known to be associated with CHARGE syndrome (it is mutated in more than 90% of subjects), correlating with the low haploinsufficiency index of *CHD7* and the clinical outcome of DGAP239 (see Supplemental Note and Tables S3 and S4).[43]

Table 3. Genomic Localization of the Disrupted Chromosome Bands in Comparison to Karyotypically Reported Bands

Subject	Next-Gen Cytogenetic Nomenclature[40] (Short System)	G-Band	Next-Gen Band	Revised Band Range: Nucleotides (Distance)	Genes[a]	Phenotype-Associated Loci[b]
DGAP239	46,XY,t(6;8)(q13;q13)dn.arr(1-22)x2,(XY)x1. seq[GRCh37/hg19] t(6;8)(q13;q12.2)dn	6q13	6q13	6q13: 70,000,001–75,900,000 (5.9 Mb)	63	16
		8q13	8q12.2	8q12q21: 55,500,001–93,300,000 (37.8 Mb)	334	41
DGAP247	46,XY,inv(8)(q13q24.1)dn.arr(1-22)x2,(XY)x1. seq[GRCh37/hg19] inv(8)(q11.21q24.23)dn	8q13	8q11.21	8q11q21: 45,600,001–93,300,000 (47.7 Mb)	406	47
		8q24.1	8q24.23	8q24: 117,700,001–146,364,022 (28.7 Mb)	306	47
DGAP248	46,XY,t(2;13)(p13;q14)dn.arr(1-22)x2,(XY)x1. seq[GRCh37/hg19] t(2;13)(p12;q13.2)dn	2p13	2p12	2p14p12: 64,100,001–83,300,000 (19.2 Mb)	225	32
		13q14	13q13.2	13q13q21: 32,200,001–73,300,000 (41.1 Mb)	375	47
DGAP258	46,XY,inv(6)(p23q13)dn.arr(1-22)x2,(XY)x1. seq[GRCh37/hg19] inv(6)(p25.3q16.1)dn[c]	6p23	6p25.3	6p25p22: 1–30,400,000 (30.4 Mb)	679	74
		6q13	6q16.1	6q11q16: 61,000,001–105,500,000 (44.5 Mb)	293	44
DGAP259	46,XX,t(3;18;5;7)(p25;p11.2;q13.3;q32),t(9;18)(p22;q21)dn.arr(1-22,X)x2. seq[GRCh37/hg19](3,5,7,9,18)cx,der(3)t(3;7)(p24.3;q36.3)dn,der(5)t(5;7)(q14.3;q35)t(3;7)(p24.3;q36.3) t(3;18)(p26.3;p11.31)dn,der(7)t(5;7)dn, der(9)t(9;18)(p23;q21.3)dn, der(18)t(3;18)inv(18)(p11.31q21.3)t(9;18)dn	3p25	3p26.3 3p24.3	3p26p24:1–30,900,000 (30.9 Mb)	277	49
		5q13.3	5q14.3	5q12q14: 58,900,001–92,300,000 (33.4 Mb)	323	358
		7q32	7q35 7q36.3	7q31q36: 107,400,001–159,138,663 (51.8 Mb)	693	80
		9p22	9p23	9p23p21: 9,000,001–33,200,000 (24.2 Mb)	181	33
		18p11.2	18p11.31	18p11: 1–17,200,000 (17.2 Mb)	192	29
		18q21	18q21.3	18q21: 43,500,001–61,600,000 (18.1 Mb)	172	33
DGAP268	46,XY,inv(10)(p13q24)dn.arr(1-22)x2,(XY)x1. seq[GRCh37/hg19]inv(10)(p12.2p12.31)(p12.2q23.32)dn	10p13	10p12.31 10p12.2	10p14p12: 6,600,001–29,600,000 (23 Mb)	233	26
		10q24	10q23.32	10q23q25: 82,000,001–119,100,000 (37.1 Mb)	467	84
DGAP285	46,Y,inv(X)(p11.2q28).arr(1-22)x2,(XY)x1. seq[GRCh37/hg19] inv(X)(p11.2q28)	Xp11.2	Xp11.21	Xp11.2: 46,400,001–58,100,000 (11.7 Mb)	274	65
		Xq28	Xq28	Xq28: 147,100,001–155,270,560 (8.2 Mb)	192	63
DGAP288	46,XX,t(6;17)(q13;q21)dn.arr(1-22,X)x2. seq[GRCh37/hg19] t(6;17)(q21;q24.3)dn	6q13	6q21	6q11q21: 61,000,001–114,600,000 (53.6 Mb)	404	57
		17q21	17q24.3	17q11q24: 24,000,001–70,900,000 (46.9 Mb)	1,032	138
DGAP290	46,XY,t(2;7)(q33;q32)dn.arr(1-22)x2,(XY)x1. seq[GRCh37/hg19](2,7)cx, der(2)t(2;7)(q32.3;q33) inv(7)(q33q33)dn,der(7)t(2;7)dn	2q33	2q32.3	2q32q34: 183,000,001–215,300,000 (32.3 Mb)	313	51
		7q32	7q33	7q31q33: 107,400,001–138,200,000 (30.8 Mb)	291	49
DGAP295	46,XY,t(2;11)(p13.1;p15.5)dn.arr(1-22)x2,(XY)x1. seq[GRCh37/hg19](2,11)cx,der(2)inv(11)(p15.5)inv(11)(p15.5) t(2;11)(p13.3;p15.5)dn,der(11)t(2;11)dn	2p13.1	2p13.3	2p13: 68,600,001–75,000,000 (6.4 Mb)	133	32
		11p15.5	11p15.5	11p15.5: 1–2,800,000 (2.8 Mb)	114	31

[a]Number of genes for the presented nucleotide range (NCBI Map Viewer, annotation release 105 [GrCh37.p13]).
[b]OMIM Phenotypic Series-specific entries for the presented nucleotide range (June 9, 2015).
[c]Cryptic paternal inversion is not included.

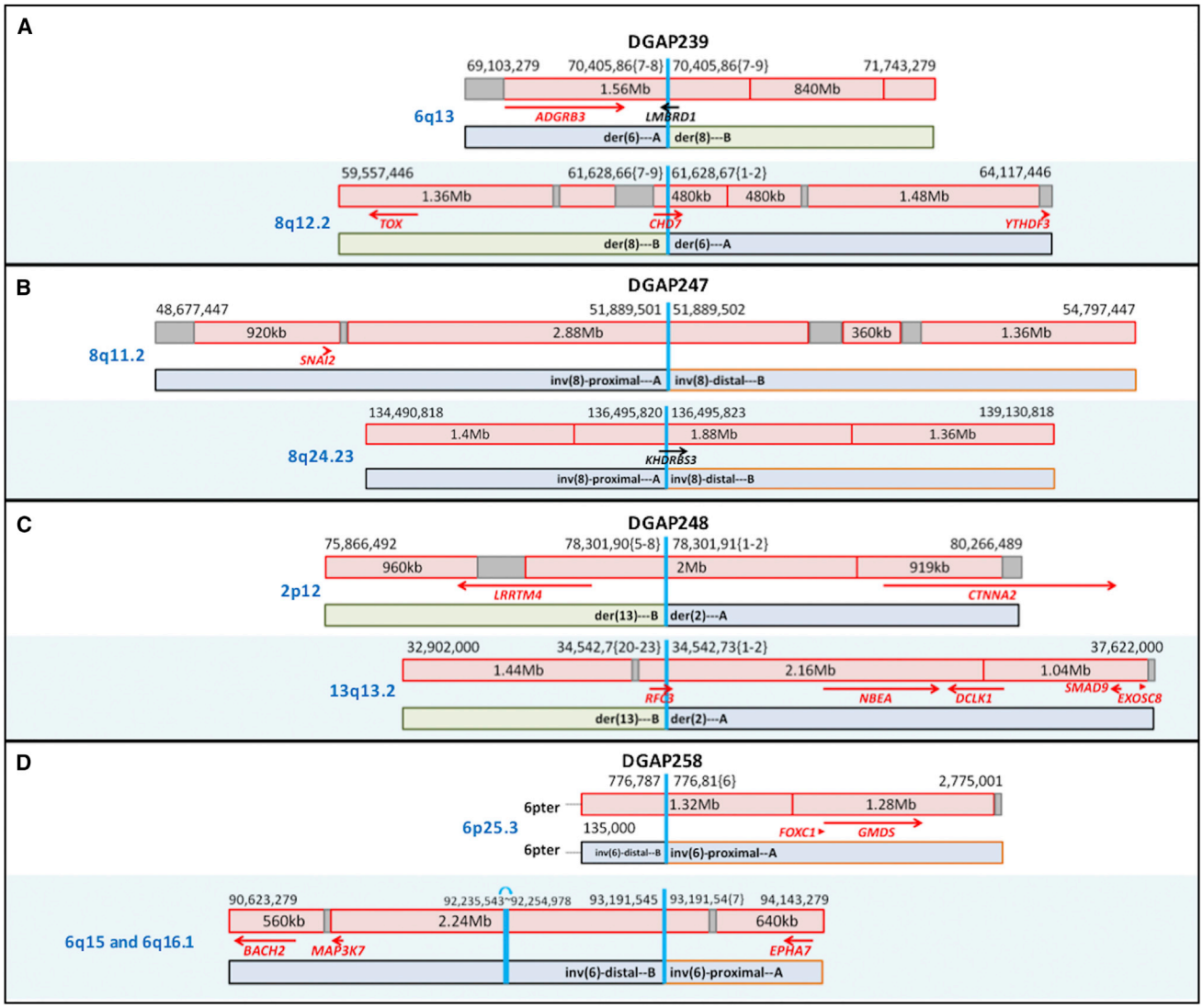

Figure 2. Diagrams of DGAP239, DGAP247, DGAP248, and DGAP258 Rearrangements
Schematic diagrams of the breakpoints of DGAP239 (A), DGAP247 (B), DGAP248 (C), and DGAP258 (D) in relation to their TAD (red box) and TBR (dark-red vertical line if 0 bp or gray box if greater than 0 bp) annotations (genes in red: haploinsufficiency index < 10%).

DGAP247

DGAP247 (46,XY,inv(8)(q13q24.1)dn.arr(1-22)x2,(XY)x1.seq[GRCh37/hg19] inv(8)(q11.21q24.23)dn) had normal prenatal findings without complications during the perinatal period. At 31 months of age, he continues to be healthy. Sequencing of the prenatal DNA sample identified inversion breakpoints (designated as inv(8)(q13q24.1) by karyotyping) within a non-genic region at 8q11.2 and disruption of *KHDRBS3* (MIM: 610421) at 8q24.23 (Figure 2B and Table 4). Although *KHDRBS3* has a borderline haploinsufficiency index and showed decreased RNA expression in the prenatal sample (see Supplemental Note, Figures S1 and S2, and Tables S5 and S6), it is not reported to be associated with a developmental role and/or abnormal phenotype, and no additional genes located in the rearranged TADs have been implicated in a phenotype or developmental role, correlating with the normal clinical phenotype.

DGAP248

DGAP248 (46,XY,t(2;13)(p13;q14)dn.arr(1-22)x2,(XY)x1.seq[GRCh37/hg19] t(2;13)(p12;q13.2)dn) had normal first-trimester screening. At 19.4 weeks, the pregnancy was terminated before the sequencing results were available. Sequencing of the prenatal DNA sample identified translocation breakpoints (designated as t(2;13)(p13;q14) by karyotyping) within a non-genic region at 2p12 and disrupting *RFC3* (MIM: 600405) at 13q13.2 (Figure 1C). The 2p12 breakpoint is located within a TAD that includes *LRRTM4* (MIM: 610870), a gene with a low haploinsufficiency index and no reported abnormal phenotypic association. However, structure and expression profiles of *LRRTM* mRNAs in mice suggest a role in development and maintenance of the vertebrate nervous system.[44] *RFC3* has a low haploinsufficiency index and showed decreased RNA expression in the prenatal sample (Figure S3).[36] In addition, *NBEA* (MIM: 6084889), a candidate autism gene with a low

Table 4. DGAP239, DGAP247, DGAP248 and DGAP258: Significant Protein-Coding Genes Surrounding the Breakpoints according to TADs and Convergent Genomic Evidence

Gene	Nucleotides (GRCh37/hg19)	Description	OMIM[37]	OMIM Morbid[37]	DDG2P[39]	HI (%)[36]	Notes
DGAP239: 6q13 Breakpoints on Rearrangement_A (70,405,86{7-8}) and Rearrangement_B (70,405,86{7-9})							
ADGRB3	69,345,259–70,099,403	adhesion G protein-coupled receptor B3	602684	–	–	3.02	no reported phenotype association; homologous to *ADGRB1*, an angiogenesis inhibitor that is a candidate for involvement in development of glioblastoma[41]
LMBRD1 (disrupted)	70,385,694–70,507,003	LMBR1 domain containing 1	612625	+	+	12.92	biallelic loss of function (autosomal recessive) associated with methylmalonic aciduria and homocystinuria, cblF type[42] (no phenotypic overlap with DGAP239)
DGAP239: 8q12.2 Breakpoints on Rearrangement_A (61,628,67{1-2}) and Rearrangement_B (61,628,66{7-9})							
CHD7 (disrupted)	61,591,337–61,779,465	chromodomain helicase DNA binding protein 7	608892	+	+	2.4	haploinsufficiency (autosomal dominant, monoallelic) reported to be associated with CHARGE syndrome, such that mutations in >90% of subjects meet diagnostic criteria of CHARGE syndrome[43] (consistent with the clinical diagnosis of CHARGE syndrome during the postnatal period of DGAP239)
DGAP247: 8q11.2 Breakpoints on Rearrangement_A (51,889,501) and Rearrangement_B (51,889,502)							
No significant gene within the same TAD as the breakpoints							
DGAP247: 8q24.23 Breakpoints on Rearrangement_A (136,495,820) and Rearrangement_B (136,495,823)							
KHDRBS3	136,469,700–136,668,965	KH domain containing, RNA binding, signal transduction associated 3	610421	–	–	10.52	no reported phenotype association
DGAP248: 2p12 Breakpoints on Rearrangement_A (78,301,91{1-2}) and Rearrangement_B (78,301,90{8-5})							
LRRTM4	76,974,845–77,820,445	leucine rich repeat transmembrane neuronal 4	610870	–	–	7.26	no reported phenotype association; structure and expression profile of *LRRTM* mRNAs in mice suggest role in development and maintenance of the vertebrate nervous system[44]
DGAP248: 13q13.2 breakpoints on Rearrangement_A (34,542,73{2-1}) and Rearrangement_B (34,542,7{20-23})							
RFC3 (disrupted)	34,392,186–34,540,695	replication factor C subunit 3	600405	–	–	4.93	no reported phenotype association
NBEA	35,516,424–36,247,159	neurobeachin	6084889	–	–	6.83	disrupted in a subject with a de novo translocation and idiopathic autism,[45] and haploinsufficiency causes autism-like behaviors in animal models[46,47]
DGAP258: 6p25.3 Breakpoints on Rearrangement_A (776,81{6}) and Rearrangement_B (776,787)							
No significant gene within the same TAD as the breakpoints							
DGAP258: 6q16.1 Breakpoints on Rearrangement_A (93,191,54{7}) and Rearrangement_B (93,191,545)							
MAP3K7	91,223,292–91,296,764	mitogen-activated protein kinase kinase kinase 7	602614	–	–	2.75	no reported phenotype association

Abbreviations are as follows: DDG2P, Developmental Disorders Genotype-to-Phenotype database; and HI, haploinsufficiency index.

haploinsufficiency score,[45,46] is located within the same 2.16 Mb TAD and 973 kb downstream of the breakpoints (Figure 2C and Table 4). Given the presence of two genes with low haploinsufficiency indices—one associated with a phenotype and located within the 13q13.2 rearrangement TAD (*NBEA*) and the other implicated in nervous

system development and located within the 2p12 rearrangement TAD (*LRRTM4*)—but the lack of strong evidence for a phenotypic correlation, these results are interpreted as "unknown clinical significance. Clinical follow-up was not possible because the pregnancy was terminated (see Supplemental Note and Tables S7 and S8). Of note, the pregnancy was terminated prior to communication of the sequencing results on the basis of an informed decision after karyotyping, CMA, and genetic counseling.

DGAP258

DGAP258 (46,XY,inv(6)(p23q13)dn.arr(1-22)x2,(XY)x1.seq[GRCh37/hg19] inv(6)(p25.3q16.1)dn(q15q15)pat or 46,XY,inv(6)(p23q13)dn.arr(1-22)x2,(XY)x1.seq[GRCh37/hg19] inv(6)(p25.3q16.1)dn,inv(6)(q15q15)pat) was a monozygotic twin pregnancy, and amniocentesis was performed as a result of abnormal first-trimester serum screening. Other than minor complications due to a twin pregnancy, there were no abnormal clinical findings during the perinatal period. At 2.5 years of age, the twins continue to be healthy. Sequencing of the prenatal DNA sample identified inversion breakpoints (designated as inv(6)(p23q13) by karyotyping) within non-genic regions at both 6p25.3 and 6q16.1. In addition, a paternally inherited cryptic non-genic rearrangement at 6q15 was detected (Figure 2D and Table 4). Because of the length of the sequencing reads, it was not possible to determine whether both of the breakpoints on 6q reside in the same paternally inherited chromosome; however, given their relative proximity and localization within the same 2.21 Mb TAD, this is a likely possibility. Analysis of protein-coding genes localized in the same TAD as the breakpoints did not reveal any additional genes associated with an abnormal phenotype or a developmental role, correlating with the normal clinical phenotype of DGAP258 (see Supplemental Note and Tables S9 and S10).

DGAP259

DGAP259[31] (46,XX,t(3;18;5;7)(p25;p11.2;q13.3;q32),t(9;18)(p22;q21)dn.arr(1-22,X)x2.seq[GRCh37/hg19](3,5,7,9,18)cx,der(3)t(3;7)(p24.3;q36.3)dn,der(5)t(5;7)(q14.3;q35)t(3;7)(p24.3;q36.3)t(3;18)(p26.3;p11.31)dn,der(7)t(5;7)dn,der(9)t(9;18)(p23;q21.3)dn,der(18)t(3;18)inv(18)(p11.31q21.3)t(9;18)dn) had abnormal prenatal findings of bilateral ventriculomegaly and colpocephaly with partial agenesis of the corpus callosum and a complex amniotic fluid karyotype designated as 46,XX,t(3;18;5;7)(p25;p11.2;q13.3;q32),t(9;18)(p22;q21)dn. The pregnancy was terminated at 22 weeks as a result of the abnormal findings. Sequencing of the prenatal DNA sample identified nine rearrangement sequences located at 3p26.3, 3p24.3, 5q14.3, 7q35, 7q36.3, 9p23, 18p11.31, and 18q21.3 with small deletions and duplications less than 1 kb (Figure 3 and Table 5). Among six disrupted protein-coding genes, *TBC1D5* (MIM: 615740) and *CNTNAP2* (MIM: 604569) reside in the vicinity of well-known genome-organizer- and chromatin-regulator-encoding regions—*SATB1* (MIM: 602075)[50] and *EZH2* (MIM: 601573)[61] at 3p24.3 and 7q35, respectively—which might be relevant to the complex chromosomal aberration of DGAP259 (all four of these genes are predicted to have low haploinsufficiency indices). Breakpoints at 7q36.3 disrupt the regulatory region of *SHH*, which has a low haploinsufficiency index. Monoallelic disruption of this *SHH* regulatory region is associated with holoprosencephaly,[26] which is consistent with the cerebral malformation phenotype of DGAP259. Breakpoints at 5q14.3 are located within the same TAD as *MEF2C* (MIM: 600662), another gene that has a low haploinsufficiency index and is associated with cerebral malformation and hypoplastic corpus callosum,[47,54] as observed in DGAP259 (see Supplemental Note and Tables S11–S18).

DGAP268

DGAP268 (46,XY,inv(10)(p13q24)dn.arr(1-22)x2,(XY)x1.seq[GRCh37/hg19] inv(10)(p12.2p12.31)(p12.2q23.32)dn) had abnormal nuchal translucency detected in the first trimester, and there were no complications during the perinatal period. At 1 year of age, he continues to be healthy. Sequencing of the prenatal DNA sample identified a complex inversion with breakpoints (designated as inv(10)(p13q24) by karyotyping) within non-genic regions at 10p12.31 and 10p12.2 and disruption *CPEB3* (MIM: 610606) at 10q23.32 (Figure 4A and Table 6). *CPEB3* does not have a low haploinsufficiency index and does not have any abnormal phenotypic association. Analysis of protein-coding genes localized in the same TAD as the breakpoints also did not reveal any genes associated with an abnormal phenotype, correlating with the normal clinical phenotype of DGAP268 (see Supplemental Note and Tables S19–S21).

DGAP285

DGAP285 (46,Y,inv(X)(p11.2q28).arr(1-22)x2,(XY)x1.seq[GRCh37/hg19] inv(X)(p11.21q28)) showed abnormal prenatal imaging findings, including hydrocephalus, starting at 22.5 weeks and fetal demise at 31.4 weeks after decreased fetal movements. Sequencing of the prenatal DNA sample identified inversion breakpoints (designated as inv(X)(p11.2q28) by karyotyping) disrupting *FAM104B* at Xp11.21 and within a non-genic region at Xq28 (Figure 4B and Table 6). Breakpoints at Xq28 disrupt a TBR, which could result in genomic rewiring of the surrounding TADs and TBRs. *MTM1* (MIM: 300415) is an X-linked recessively inherited gene associated with centronuclear myopathy (MIM: 310400), a prenatal-onset fatal disease with clinical findings including decreased fetal movements, hydrocephalus, and stillbirth.[73–75] *MTM1* is located in a TBR upstream of the TBR at the Xq28 rearrangement, and therefore dysregulation of *MTM1* might contribute to the phenotype of DGAP285 (see Supplemental Note and Tables S22 and S23).

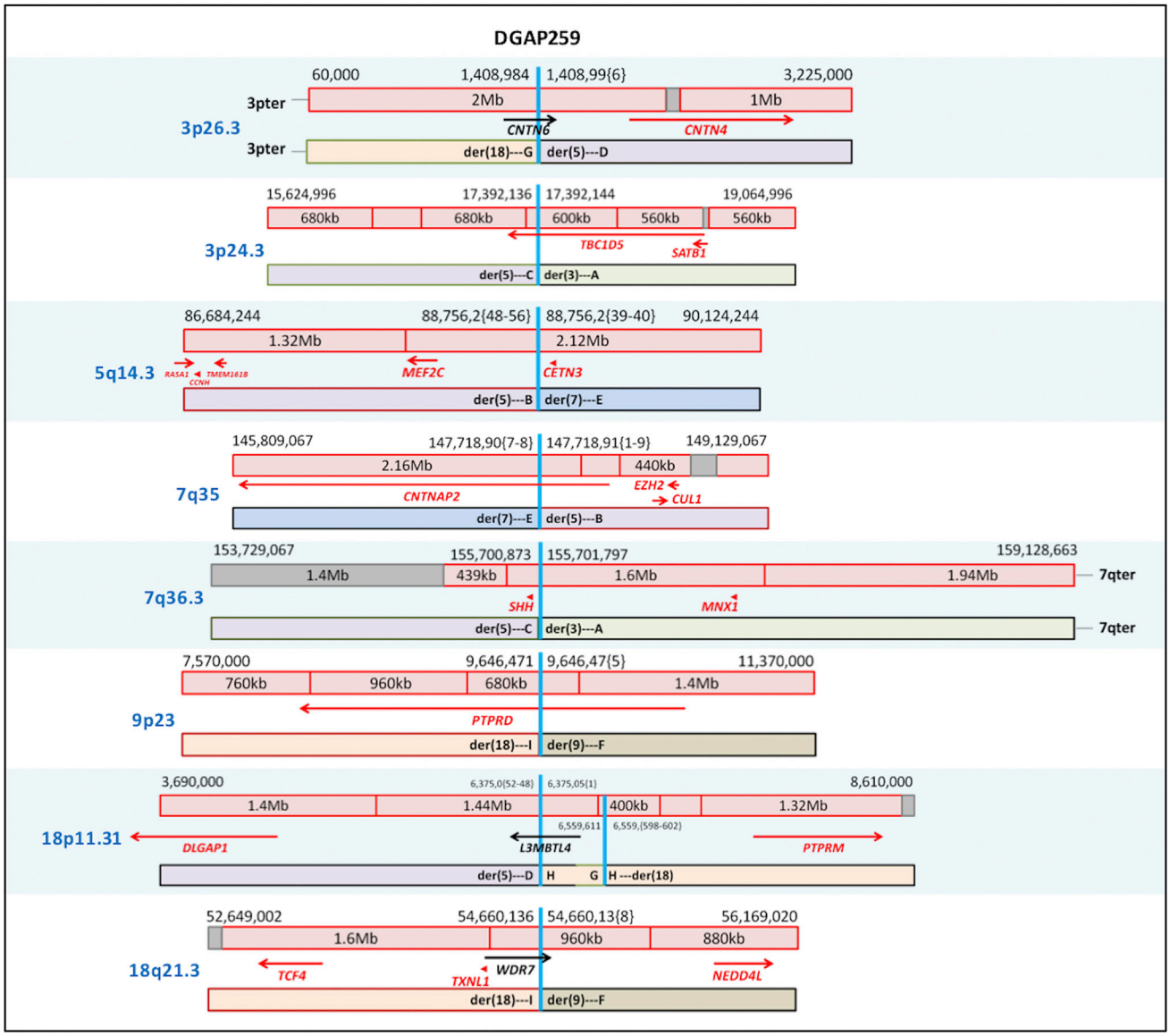

Figure 3. Diagrams of DGAP259 Rearrangements
Schematic diagrams of the breakpoints of DGAP259 in relation to their TAD (red box) and TBR (dark-red vertical line if 0 bp or gray box if greater than 0 bp) annotations (genes in red: haploinsufficiency index < 10%).

DGAP288

DGAP288 (46,XX,t(6;17)(q13;q21)dn.arr(1-22,X)x2.seq [GRCh37/hg19] t(6;17)(q21;q24.3)dn) had cystic hygroma at 11.1 weeks, followed by prenatal imaging findings consistent with Pierre Robin sequence, which were confirmed during the postnatal period. Sequencing of the prenatal DNA sample identified translocation breakpoints (designated as t(6;17)(q13;q21) by karyotyping) within non-genic regions at 6q21 and 17q24.3 (Figure 4C and Table 6). Breakpoints at 17q24.3 were in a 1.88 Mb TAD corresponding to an upstream *cis*-regulatory region of *SOX9* (MIM: 608160), a region known to be associated with Pierre Robin sequence as a result of dysregulation of *SOX9*, an autosomal-dominantly inherited gene with a low haploinsufficiency index.[25,28,29] The prenatal sample showed decreased RNA expression of *SOX9* (Figure 5), correlating with the clinical outcome of DGAP288 (see Supplemental Note and Tables S24 and S25).

DGAP290

DGAP290 (46,XY,t(2;7)(q33;q32)dn.arr(1-22)x2,(XY)x1.seq[GRCh37/hg19](2,7)cx,der(2)t(2;7)(q32.3;q33)inv(7)(q33q33)dn,der(7)t(2;7)dn) was a high-risk pregnancy according to first-trimester screening, which showed normal imaging up to 18 weeks. The parents decided to terminate the pregnancy at 23 weeks because of uncertainty of the clinical significance of the balanced rearrangement. Sequencing of the prenatal DNA sample identified translocation breakpoints (designated as t(2;7)(q33;q32) by karyotyping) disrupting *HECW2* at 2q32.3 and *NUP205*

Table 5. DGAP259: Significant Protein-Coding Genes Surrounding the Breakpoints according to TADs and Convergent Genomic Evidence

Gene	Nucleotides (GRCh37/hg19)	Description	OMIM[37]	OMIM Morbid[37]	DDG2P[39]	HI (%)[36]	Notes
3p26.3 Breakpoints on Rearrangement_D (1,408,99{6}) and Rearrangement_G (1,408,984)							
CNTN6 (disrupted)	1,134,260–1,445,901	contactin 6	607220	–	–	39.69	no reported phenotype association; neural adhesion molecule[48]
CNTN4	2,140,497–3,099,645	contactin 4	607280	–	–	6.9	disrupted in a subject with a 3p deletion syndrome (autosomal-dominant) phenotype[49] (cerebral and renal malformation phenotype of DGAP259)
3p26.3 Breakpoints on Rearrangement_D (1,408,99{6}) and Rearrangement_G (1,408,984)							
TBC1D5 (disrupted)	17,198,654–18,486,309	TBC1 domain family member 5	615740	–	–	5.84	no reported phenotype association
SATB1[a]	18,386,879–18,487,080	SATB homeobox 1	602075	–	–	2.15	global genome organizer[50,51] (complex chromosomal rearrangement of DGAP259); role in neuronal plasticity of cortical neurons and regulation of key neuronal genes[52,53] (cerebral malformation phenotype of DGAP259)
5q14.3 Breakpoints on Rearrangement_B (88,756,2{48-56}) and Rearrangement_E (88,756,2{39-40})							
MEF2C	88,013,975–88,199,922	myocyte enhancer factor 2C	600662	+	+	0.26	haploinsufficiency (autosomal dominant, monoallelic) associated with mental retardation, stereotypic movements, epilepsy, and cerebral malformations (MIM: 613443)[47,54] (cerebral malformation and hypoplastic corpus callosum phenotype of DGAP259); role in synaptic plasticity and hippocampal-dependent learning and memory[55] (9p23 breakpoints of DGAP259 disrupt *PTPRD1* with similar role)
CETN3	89,688,078–89,705,603	centrin 3	602907	–	–	5.94	present in centrosomes and important role in early cleavage of frog embryos[56] (complex chromosomal rearrangement of DGAP259)
7q35 Breakpoints on Rearrangement_B (147,718,91{1-9}) and Rearrangement_E (147,718,90{7-8})							
CNTNAP2 (disrupted)	145,813,453–148,118,090	contactin associated protein-like 2	604569	+	+	4.94	susceptibility to autism type 15;[57] homozygous or compound-heterozygous mutations cause Pitt-Hopkins-like syndrome 1 (MIM: 610042)[58] (cerebral malformation phenotype of DGAP259; 18q21 breakpoints are one TAD downstream of *TCF4*, associated with Pitt-Hopkins syndrome)
CUL1[a]	148,395,006–148,498,128	cullin 1	603134	–	–	4.3	regulates the mammalian G1/S transition[59]
EZH2[a]	148,504,475–148,581,413	enhancer of zeste 2 polycomb repressive complex 2 subunit	601573	+	+	3.07	has a critical role during normal and perturbed development of the hematopoietic and central nervous systems,[60] maintains homeotic gene repression, and is thought to control gene expression by regulating chromatin[61] (cerebral malformation and complex chromosomal rearrangement of DGAP259)

(*Continued on next page*)

Table 5. *Continued*

Gene	Nucleotides (GRCh37/hg19)	Description	OMIM[37]	OMIM Morbid[37]	DDG2P[39]	HI (%)[36]	Notes
7q36.3 Breakpoints on Rearrangement_A (155,701,797) and Rearrangement_C (155,700,873)							
SHH	155,592,680–155,604,967	sonic hedgehog	600725	+	+	0.66	haploinsufficiency (autosomal dominant, monoallelic) associated with HPE3,[62] which has a long-range regulation-associated phenotype[63] (cerebral malformation phenotype of DGAP259)
9p23 Breakpoints on Rearrangement_F (9,646,47{5}) and Rearrangement_I (9,646,471)							
PTPRD (disrupted)	8,314,246–10,612,723	protein tyrosine phosphatase, receptor type D	601598	–	–	0.14	homozygous microdeletion causes trigonocephaly, hearing loss, and intellectual disability, which overlap the autosomal-dominant 9p deletion syndrome[64] (cerebral malformation phenotype of DGAP259); role in synaptic plasticity and hippocampal-dependent learning and memory[65] (5q14.3 breakpoints are within the same TAD as *MEF2C* with similar role)
18p11.31 Breakpoints on Rearrangement_D (6,375,05{1}), Rearrangement_G (6,559,611), and Rearrangement_H (6,375,0{52-48} and 6,559,{598-602})							
L3MBTL4 (disrupted)	5,954,705–6,415,236	L(3)Mbt-like 4 (*Drosophila*)	–	–	–	59.07	no reported phenotype association
18q21.3 Breakpoints on Rearrangement_F (54,660,13{8}) and Rearrangement_I (54,660,136)							
TCF4[a]	52,889,562–53,332,018	transcription factor 4	602272	+	+	0.38	haploinsufficiency (autosomal dominant, monoallelic) is associated with Pitt-Hopkins syndrome[66] (cerebral malformation phenotype of DGAP259, 7q35 breakpoints disrupt *CNTNAP2*, related to Pitt-Hopkins-like syndrome[58])
WDR7 (disrupted)	54,318,574–54,698,828	WD repeat domain 7	613473	–	–	14.85	no reported phenotype association; localized to synaptic vesicles in rat and mouse brain[67]
NEDD4L[a]	55,711,599–56,068,772	neural precursor cell expressed, developmentally down-regulated 4-like, E3 ubiquitin protein ligase	606384	–	–	8.66	regulator of renal sodium channels; involved in induction of mesoendodermal fates in mouse embryonic stem cells[68] (renal malformation phenotype of DGAP259)

Abbreviations are as follows: DDG2P, Developmental Disorders Genotype-to-Phenotype database; HI, haploinsufficiency index; and HPD3, holoprosencephaly type 3.
[a]Although not located within the same hESC TAD[18] as the breakpoint, these genes might be relevant to the phenotype of DGAP259 given the complexity of the rearrangement.

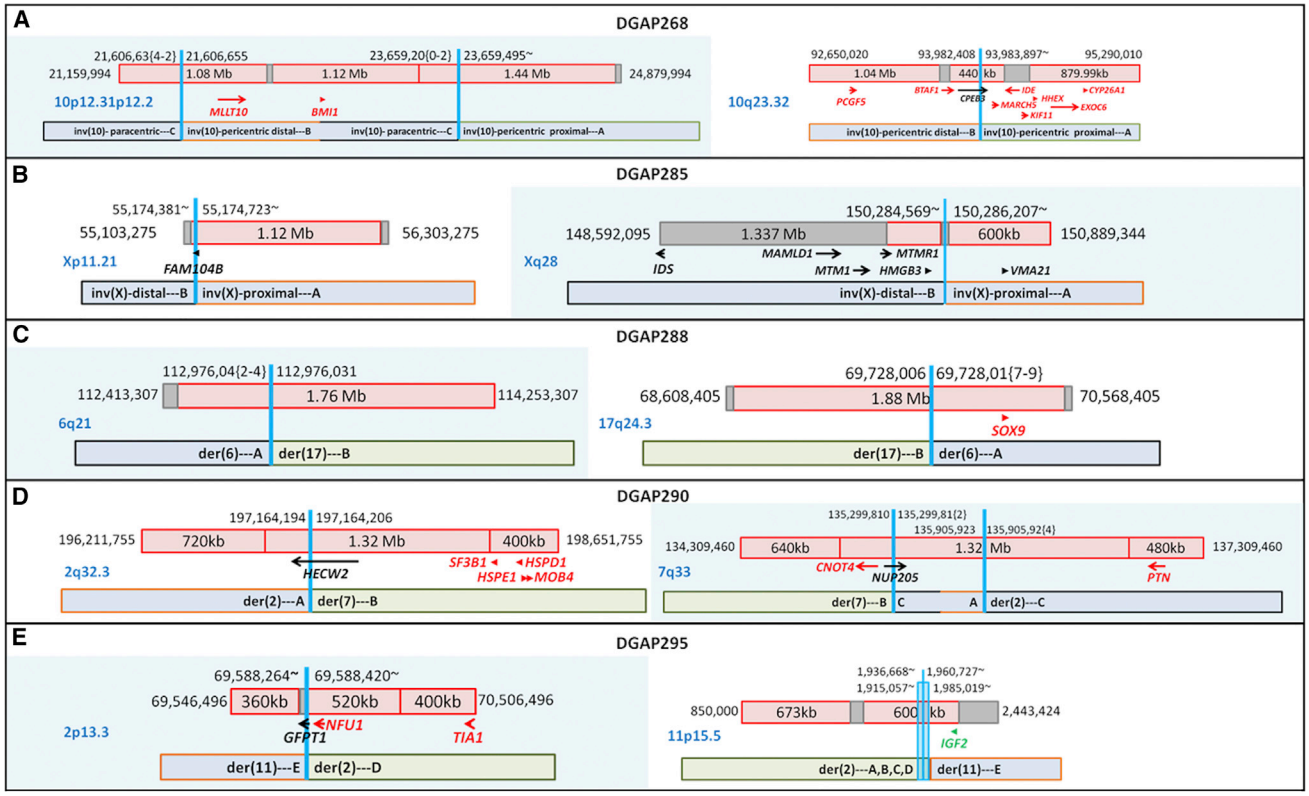

Figure 4. Diagrams of DGAP268, DGAP285, DGAP288, DGAP290, and DGAP290 Rearrangements
Schematic diagrams of the breakpoints of DGAP268 (A), DGAP285 (B), DGAP288 (C), DGAP290 (D), and DGAP290 (E) in relation to their TAD (red box) and TBR (dark-red vertical line if 0 bp or gray box if greater than 0 bp) annotations (genes in red: haploinsufficiency index < 10%; green: imprinted).

(MIM: 614352) at 7q33 and an additional non-genic disruption at 7q33 (Figure 4D and Table 6). Neither disrupted gene had a low haploinsufficiency index, and analysis of protein-coding genes in the same TAD as the breakpoints did not reveal any genes associated with an abnormal phenotype. These results are interpreted as "unknown clinical significance, likely to be benign"; however, clinical correlation was not possible because the pregnancy was terminated (see Supplemental Note and Tables S26 and S27).

DGAP295

DGAP295 (46,XY,t(2;11)(p13.1;p15.5)dn.arr(1-22)x2,(XY)x1.seq[GRCh37/hg19](2,11)cx,der(2)inv(11)(p15.5)inv(11)(p15.5)t(2;11)(p13.3;p15.5)dn,der(11)t(2;11)dn) had abnormal first-trimester screening, which showed an abnormal prenatal imaging finding of growth restriction starting from 19 weeks, and weighed 450 g upon delivery at 31 weeks. Sequencing of the prenatal DNA sample identified translocation breakpoints (designated as t(2;11)(p13.1;p15.5) by karyotyping) disrupting *GFPT1* (MIM: 138292) at 2p13.3 and multiple non-genic regions at 11p15.5 within a 70 kb distribution (Figure 4E and Table 6). The complex breakpoints at 11p15.5 are within the same 600 kb TAD as *IGF2* (MIM: 147470), an imprinted region known to be associated with growth restriction with distinctive facies (GRDF [MIM: 616489])[71] and Silver-Russell syndrome (MIM: 180860),[72] consistent with the growth restricted phenotype of DGAP295 (see Supplemental Note and Tables S28 and S29).

Discussion

We report whole-genome sequencing of ten prenatal subjects with balanced chromosomal rearrangements with "normal" CMA results and their phenotypic interpretation through publicly available resources. Each subject has contributed uniquely to our experience in the evolution of this approach to a new standard of care in prenatal diagnosis by providing further insight into prognosis through incorporation of an understanding of the regulatory genome (Table 7).

In the evaluation of the pathogenic outcomes of balanced rearrangements, disruption or dysregulation of a single allele is of particular significance when it involves a region known to be hemizygous for X-linked traits, haploinsufficient (autosomal dominant), or imprinted and associated with an abnormal phenotype. Next-generation sequencing can identify the disrupted regions at the nucleotide level; however, predicting the dysregulation of the genes in the vicinity of the breakpoints is more challenging. Advances in the understanding of large-scale regulatory chromatin

Table 6. DGAP268, DGAP285, DGAP288, DGAP290, and DGAP295: Significant Protein-Coding Genes Surrounding the Breakpoints according to TADs and Convergent Genomic Evidence

Gene	Nucleotides (GRCh37/hg19)	Description	OMIM[37]	OMIM Morbid[37]	DDG2P[39]	HI (%)[36]	Notes
DGAP268: 10p12.31 Breakpoints on Rearrangement_B (21,606,655) and Rearrangement_C (21,606,63{4-2})							
No significant gene within the same TAD as the breakpoints							
DGAP268: 10p12.2 Breakpoints on Rearrangement_A (23,659,495~) and Rearrangement_C (23,659,20{0-2})							
No significant gene within the same TAD as the breakpoints							
DGAP268: 10q23.32 Breakpoints on Rearrangement_A (93,983,897~) and Rearrangement_B (93,982,408)							
CPEB3 (disrupted)	93,806,449–94,050,844	cytoplasmic polyadenylation element binding protein 3	610606	–	–	12.96	no reported phenotype association
DGAP285: Xp11.21 Breakpoints on Rearrangement_A (55,174,723~) and Rearrangement_B (55,174,381~)							
FAM104B (disrupted)	55,169,535–55,187,743	family with sequence similarity 104 member B	–	–	–	93.08	no reported phenotype association
DGAP285: Xq28 Breakpoints on Rearrangement_A (150,286,207~) and Rearrangement_B (150,284,569~)							
MTM1	149,737,069–149,841,795	myotubularin 1	300415	+	+	12.54	hemizygous loss of function (X-linked recessive) associated with X-linked myotubular myopathy[69] (overlapping the phenotype of DGAP285)
DGAP288: 6q21 Breakpoints on Rearrangement_A (112,976,04{2-4}) and Rearrangement_B (112,976,031)							
No significant gene within the same TAD as the breakpoints							
DGAP288: 17q24.3 Breakpoints on Rearrangement_A (69,728,01{7-9}) and Rearrangement_B (69,728,006)							
SOX9	70,117,161–70,122,561	SRY-box 9	608160	+	+	0.56	haploinsufficient (autosomal dominant, monoallelic) long-range *cis*-regulation associated with Pierre Robin sequence[28] (overlapping the phenotype of DGAP288)
DGAP290: 2q32.3 Breakpoints on Rearrangement_A (197,164,194) and Rearrangement_B (197,164,206)							
HECW2 (disrupted)	197,059,094–197,458,416	HECT, C2, and WW domain containing E3 ubiquitin protein ligase 2	–	–	–	18.5	no reported phenotype association
DGAP290: 7q33 Breakpoints on Rearrangement_A (135,905,923), Rearrangement_B (135,299,810), and Rearrangement_C (135,299,81{2} and 135,905,92{4})							
NUP205 (disrupted)	135,242,667–135,333,505	nucleoporin 205	614352	–	–	11.41	no reported phenotype association

(*Continued on next page*)

Table 6. *Continued*

Gene	Nucleotides (GRCh37/hg19)	Description	OMIM[37]	OMIM Morbid[37]	DDG2P[39]	HI (%)[36]	Notes
DGAP295: 2p13.3 Breakpoints on Rearrangement_D (69,588,420~) and Rearrangement_E (69,588,264~)							
GFPT1 (disrupted)	69,546,905–69,614,382	glutamine-fructose-6-phosphate transaminase 1	138292	+	–	22.36	biallelic loss of function (autosomal recessive) associated with congenital myasthenia type 12[70] (no overlap with the phenotype of DGAP295)
DGAP295: 11p15.5 Breakpoints on Rearrangement_A (1,915,057~ and 1,936,993~), Rearrangement_B (1,960,727~ and 1,936,668~), Rearrangement_C (1,915,843~ and 1,961,361~), Rearrangement_D (1,984,895~), and Rearrangement_E (1,985,019~)							
IGF2	2,150,342–2,170,833	insulin-like growth factor 2	147470	+	+	79.01	imprinted loss of function (epimutation) associated with GRDF[71] and Silver-Russell syndrome[72] (overlapping the phenotype of DGAP295)

Abbreviations are as follows: DDG2P, Developmental Disorders Genotype-to-Phenotype database; GRDF, growth restriction with distinctive facies; and HI, haploinsufficiency index.

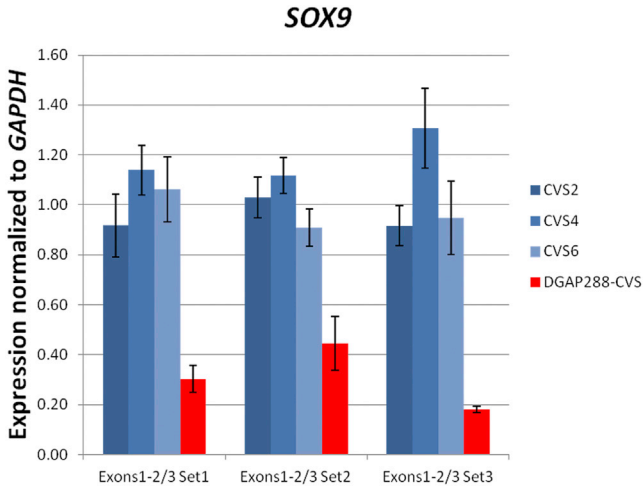

Figure 5. *SOX9* Expression of DGAP288
Decreased expression of *SOX9* in the chorionic villus sample (CVS) of DGAP288 in comparison to three CVS controls (three different primer sets were used for the expression assessment of exons 1 and 2 out of 3, normalized to *GAPDH*). Error bars represent the SE of the normalized ratios.

domains (TADs) contribute to overcoming this obstacle. A recent study analyzing the *WNT6-IHH-EPHA4-PAX3* locus and three related congenital genetic disorders has provided multiple layers of evidence for the significance of these megabase-sized regulatory domains and their contribution to abnormal phenotypes through genomic rewiring of the regulatory boundaries resulting from structural rearrangements.[20] It is well established that the *cis*-regulatory elements for many key developmental genes can extend beyond the transcription unit in the range of 120 kb to 1.5 Mb,[15–17,76,77] which could be explained by these regulatory associations. Therefore, we analyzed the aforementioned characteristics (hemizygosity, haploinsufficiency, and imprinting) of the disrupted genes at the breakpoints, as well as the protein-coding genes located in the regulatory domains and boundaries (TADs and TBRs, respectively) associated with the breakpoints to identify the dysregulated regions. Then, we evaluated the phenotypic and developmental significance of these genes of interest. None of the three subjects with normal outcomes (DGAP247, DGAP258, and DGAP268) had disrupted genes or were predicted to have dysregulated genes involved with an abnormal phenotype. Among five subjects with abnormal outcomes, one (DGAP239) had a disrupted syndromic gene with a low haploinsufficiency index, one (DGAP285) had a disrupted TBR and was predicted to have a dysregulated X-linked recessively inherited syndromic gene, one (DGAP288) had a dysregulated gene involved with an abnormal phenotype, one (DGAP295) was predicted to have a dysregulated imprinted gene involved with a syndrome, and lastly, in one chromothripsis-affected subject (DGAP259), multiple genes associated with CNS malformations and genomic organization were disrupted and predicted to be dysregulated. All showed abnormal phenotypes overlapping the

Table 7. Lessons Learned: Next-Generation Sequencing of Ten Prenatal Subjects

Subject	Gene(s) of Interest according to Sequencing Results	Interpretation of the Sequencing Results	Clinical Significance	Clinical Outcome
DGAP239	*CHD7* (disrupted), *LMBRD1* (disrupted)	disruption of an autosomal-dominant gene with a low haploinsufficiency index and associated with CHARGE syndrome (pathogenic) and an autosomal-recessive gene (non-contributory)	pathogenic	CHARGE syndrome
DGAP247	*KHDRBS3* (disrupted)	disruption of a single gene without pathogenicity	unknown, likely to be benign	healthy newborn
DGAP248	*LRRTM4*, *RFC3* (disrupted), *NBEA*	disruption of a gene with a low haploinsufficiency index but no reported pathogenicity; potential dysregulation of an additional gene with a low haploinsufficiency index and reported to be associated with autism-like behaviors in animal models and disrupted in a subject with idiopathic autism[45,46]	unknown	termination prior to communication of sequencing results
DGAP258	–	non-genic breakpoints with cryptic paternal inversion not at the karyotypically detected breakpoint	unknown, likely to be benign	healthy newborns
DGAP259	*CNTN6* (disrupted), *CNTN4*, *TBC1D5* (disrupted), *SATB1*, *MEF2C*, *CETN3*, *CNTNAP2* (disrupted), *CUL1*, *EZH2*, *SHH*, *PTPRD* (disrupted), *L3MBTL4* (disrupted), *TCF4*, *WDR7* (disrupted), *NEDD4L*	complex rearrangement with potential dysregulation of genes with a low haploinsufficiency index and associated with malformation in the CNS and chromatin organization	pathogenic	termination due to multiple abnormal prenatal findings (bilateral ventriculomegaly and colpocephaly with partial agenesis of the corpus callosum)
DGAP268	*CPEB3* (disrupted)	disruption of a single gene without known pathogenicity and a cryptic inversion at non-genic breakpoints	unknown, likely to be benign	healthy newborn
DGAP285	*FAM104B* (disrupted), *MTM1*	disruption of a single gene without known pathogenicity; disruption of a TBR with potential dysregulation of a gene associated with X-linked myotubular myopathy, a prenatal-onset fatal disease	unknown, likely to be pathogenic	intrauterine fetal demise (overlapping findings with X-linked myotubular myopathy include decreased fetal movements, hydrocephalus, and stillbirth)
DGAP288	*SOX9*	non-genic breakpoints with dysregulation of a gene with a low haploinsufficiency index and known to be associated with Pierre Robin sequence	pathogenic	Pierre Robin sequence
DGAP290	*HECW2* (disrupted), *NUP205* (disrupted)	disruption of two genes without known pathogenicity; non-genic cryptic inversion in one of the breakpoints	unknown, likely to be benign	termination after communication of sequencing results
DGAP295	*GFPT1* (disrupted), *IGF2*	complex rearrangement with potential dysregulation of an imprinted gene associated with Silver-Russell syndrome (pathogenic) and a recessively inherited syndromic gene (noncontributory)	pathogenic	small birth weight and failure to thrive (findings consistent with Silver-Russell syndrome)

predicted outcomes of the sequencing results. Of note, two of the five subjects with abnormal phenotypes (DGAP239 and DGAP295) had additional disrupted genes involved in autosomal-recessive syndromes and did not show any clinical features associated with these syndromes. However, in such cases, a potential "carrier" status for the relevant syndromes might be considered in future genetic counseling of the newborn if the outcome is otherwise normal. Among the two terminated pregnancies without any abnormal phenotypes prior to termination, one subject (DGAP248) is interpreted as having a rearrangement predicted to be of unknown clinical significance, and the other (DGAP290) is interpreted has having a rearrangement predicted to be likely benign.

Although karyotyping remains the standard of care for prenatal diagnosis, advances in genomic technologies are rapidly transitioning into clinical practice. Non-invasive cfDNA screening and CMA in invasive testing are increasingly popular methods in the field of prenatal genetics.[78–80] Non-invasive prenatal testing of cfDNA offers tremendous potential as a screening tool, particularly for fetal aneuploidies. Although this next-generation-sequencing-based approach has been shown to reliably demonstrate copy-number variations greater than 5 Mb,[81] it currently remains a screening method.[2,3] Current guidelines recommend offering CMA to any woman choosing to undergo prenatal invasive diagnostic testing and recommend CMA as the primary test (replacing conventional

karyotype) if the prenatal diagnostic test is performed for an indication of a structural abnormality detected by prenatal imaging studies.[33] Nonetheless, CMA cannot assess balanced rearrangements and, if performed alone in the present study, would have "missed" all five prenatal subjects with abnormal outcomes (each of whom had abnormal prenatal imaging findings), including a subject with complex chromothripsis (DGAP259).

Karyotyping remains superior to CMA for the detection of balanced rearrangements, despite its megabase-sized resolution. Next-generation sequencing using large-insert libraries provides precise delineation of the breakpoints of structural rearrangements while detecting additional high-resolution cryptic rearrangements, as well as copy-number alterations that could potentially be detected by CMA and not karyotyping. Although cfDNA screening is also a sequence-based approach, given the fragmented nature of cell-free DNA, it would be cumbersome to analyze truly balanced rearrangements with the current cfDNA technology. Another sequence-based approach in the field of prenatal genetics is whole-exome sequencing.[82,83] Although this method provides higher nucleotide-level coverage and therefore can more reliably detect nucleotide-level mutations in the exome than our large-insert library method, given the presence of non-genic breakpoints in structural rearrangements, a whole-genome paired-end sequencing approach using large-insert libraries, as presented herein, would be most useful in detecting structural rearrangements. Currently, we would recommend using this method in subjects with a normal CMA and a karyotype with a balanced rearrangement (the order of CMA and karyotyping depends on the clinical scenario). In subjects with an abnormal CMA and/or a karyotype without a balanced rearrangement that fails to explain an abnormal phenotype, our method could still be valuable for identifying cryptic rearrangements in the appropriate clinical setting. We believe next-generation sequencing technologies will eventually be proposed as a first-line diagnostic method because they can provide details on structural rearrangements that cannot be detected by either karyotyping or CMA.

As with other genomic testing methods, whole-genome sequencing also raises the issue of variants of unknown clinical significance. The topic of "unknown clinical significance" is not a new problem for the field of prenatal diagnosis, whether it be a subtle imaging finding such as mildly enlarged ventricles or the detection of a balanced chromosomal rearrangement by karyotyping. Sequencing provides additional understanding of the breakpoints involved in a balanced chromosomal rearrangement. Although this information could fundamentally influence genetic counseling, clinical management, and decision making, it could also bring additional pressure to managing unknown findings on the basis of current genomic evidence. Eventually, evolving annotation of the human genome—including the discovery of disease-associated genes or other predictors of regulatory effect, such as pathogenic increases in gene expression—along with guidelines from expert committees, could close these gaps of interpretation, as has been the case with improved clinical reporting of CMA results over the past decade.[84]

In conclusion, detecting balanced chromosomal rearrangements with whole-genome sequencing provides nucleotide-level precision incomparable to currently employed prenatal genetic-testing methods, thus enabling the regulatory genome to be evaluated in such a way that could prove invaluable in clinical interpretation.

Supplemental Data

Supplemental Data include a Supplemental Note, 3 figures, and 29 tables and can be found with this article online at http://dx.doi.org/10.1016/j.ajhg.2016.08.022.

Acknowledgments

We are grateful to the families of the subjects for their participation. We thank Christina Jabbour, Amelia Lindgren, Samantha Schilit, and Drs. Ozden Altiok Clark and Frederick Bieber for their contributions. We dedicate this article in loving memory of Dorothy Warburton, a co-author on this study and the author of an article also published in *The Journal*,[4] which has served as a foundation for the Developmental Genome Anatomy Project. This study was funded by the NIH (GM061354 to C.C.M., M.E.T., and J.F.G.; HD081256 and March of Dimes 6-FY15-255 to M.E.T.).

Received: June 19, 2016
Accepted: August 26, 2016
Published: October 13, 2016

Web Resources

DECIPHER, https://decipher.sanger.ac.uk/
DGAP, http://www.bwhpathology.org/dgap/
OMIM, http://www.omim.org

References

1. American College of Obstetricians and Gynecologists Committee on Genetics (2013). Committee Opinion No. 581: the use of chromosomal microarray analysis in prenatal diagnosis. Obstet. Gynecol. *122*, 1374–1377.
2. (2016). Practice Bulletin No. 162 Summary: Prenatal Diagnostic Testing for Genetic Disorders. Obstet. Gynecol. 127, 976–978.
3. (2016). Practice Bulletin No. 163: Screening for Fetal Aneuploidy. Obstet. Gynecol. 127, e123–e137.
4. Warburton, D. (1991). De novo balanced chromosome rearrangements and extra marker chromosomes identified at prenatal diagnosis: clinical significance and distribution of breakpoints. Am. J. Hum. Genet. *49*, 995–1013.
5. Gribble, S.M., Prigmore, E., Burford, D.C., Porter, K.M., Ng, B.L., Douglas, E.J., Fiegler, H., Carr, P., Kalaitzopoulos, D., Clegg, S., et al. (2005). The complex nature of constitutional de novo apparently balanced translocations in patients presenting with abnormal phenotypes. J. Med. Genet. *42*, 8–16.
6. De Gregori, M., Ciccone, R., Magini, P., Pramparo, T., Gimelli, S., Messa, J., Novara, F., Vetro, A., Rossi, E., Maraschio, P., et al.

(2007). Cryptic deletions are a common finding in "balanced" reciprocal and complex chromosome rearrangements: a study of 59 patients. J. Med. Genet. *44*, 750–762.
7. Sismani, C., Kitsiou-Tzeli, S., Ioannides, M., Christodoulou, C., Anastasiadou, V., Stylianidou, G., Papadopoulou, E., Kanavakis, E., Kosmaidou-Aravidou, Z., and Patsalis, P.C. (2008). Cryptic genomic imbalances in patients with de novo or familial apparently balanced translocations and abnormal phenotype. Mol. Cytogenet. *1*, 15.
8. Baptista, J., Mercer, C., Prigmore, E., Gribble, S.M., Carter, N.P., Maloney, V., Thomas, N.S., Jacobs, P.A., and Crolla, J.A. (2008). Breakpoint mapping and array CGH in translocations: comparison of a phenotypically normal and an abnormal cohort. Am. J. Hum. Genet. *82*, 927–936.
9. Higgins, A.W., Alkuraya, F.S., Bosco, A.F., Brown, K.K., Bruns, G.A., Donovan, D.J., Eisenman, R., Fan, Y., Farra, C.G., Ferguson, H.L., et al. (2008). Characterization of apparently balanced chromosomal rearrangements from the developmental genome anatomy project. Am. J. Hum. Genet. *82*, 712–722.
10. Schluth-Bolard, C., Delobel, B., Sanlaville, D., Boute, O., Cuisset, J.M., Sukno, S., Labalme, A., Duban-Bedu, B., Plessis, G., Jaillard, S., et al. (2009). Cryptic genomic imbalances in de novo and inherited apparently balanced chromosomal rearrangements: array CGH study of 47 unrelated cases. Eur. J. Med. Genet. *52*, 291–296.
11. Gijsbers, A.C., Bosch, C.A., Dauwerse, J.G., Giromus, O., Hansson, K., Hilhorst-Hofstee, Y., Kriek, M., van Haeringen, A., Bijlsma, E.K., Bakker, E., et al. (2010). Additional cryptic CNVs in mentally retarded patients with apparently balanced karyotypes. Eur. J. Med. Genet. *53*, 227–233.
12. Feenstra, I., Hanemaaijer, N., Sikkema-Raddatz, B., Yntema, H., Dijkhuizen, T., Lugtenberg, D., Verheij, J., Green, A., Hordijk, R., Reardon, W., et al. (2011). Balanced into array: genome-wide array analysis in 54 patients with an apparently balanced de novo chromosome rearrangement and a meta-analysis. Eur. J. Hum. Genet. *19*, 1152–1160.
13. Korbel, J.O., Urban, A.E., Affourtit, J.P., Godwin, B., Grubert, F., Simons, J.F., Kim, P.M., Palejev, D., Carriero, N.J., Du, L., et al. (2007). Paired-end mapping reveals extensive structural variation in the human genome. Science *318*, 420–426.
14. Talkowski, M.E., Ernst, C., Heilbut, A., Chiang, C., Hanscom, C., Lindgren, A., Kirby, A., Liu, S., Muddukrishna, B., Ohsumi, T.K., et al. (2011). Next-generation sequencing strategies enable routine detection of balanced chromosome rearrangements for clinical diagnostics and genetic research. Am. J. Hum. Genet. *88*, 469–481.
15. Sanyal, A., Lajoie, B.R., Jain, G., and Dekker, J. (2012). The long-range interaction landscape of gene promoters. Nature *489*, 109–113.
16. Bhatia, S., and Kleinjan, D.A. (2014). Disruption of long-range gene regulation in human genetic disease: a kaleidoscope of general principles, diverse mechanisms and unique phenotypic consequences. Hum. Genet. *133*, 815–845.
17. Kleinjan, D.A., and van Heyningen, V. (2005). Long-range control of gene expression: emerging mechanisms and disruption in disease. Am. J. Hum. Genet. *76*, 8–32.
18. Dixon, J.R., Selvaraj, S., Yue, F., Kim, A., Li, Y., Shen, Y., Hu, M., Liu, J.S., and Ren, B. (2012). Topological domains in mammalian genomes identified by analysis of chromatin interactions. Nature *485*, 376–380.
19. Sexton, T., and Cavalli, G. (2015). The role of chromosome domains in shaping the functional genome. Cell *160*, 1049–1059.
20. Lupiáñez, D.G., Kraft, K., Heinrich, V., Krawitz, P., Brancati, F., Klopocki, E., Horn, D., Kayserili, H., Opitz, J.M., Laxova, R., et al. (2015). Disruptions of topological chromatin domains cause pathogenic rewiring of gene-enhancer interactions. Cell *161*, 1012–1025.
21. Bhatia, S., Bengani, H., Fish, M., Brown, A., Divizia, M.T., de Marco, R., Damante, G., Grainger, R., van Heyningen, V., and Kleinjan, D.A. (2013). Disruption of autoregulatory feedback by a mutation in a remote, ultraconserved PAX6 enhancer causes aniridia. Am. J. Hum. Genet. *93*, 1126–1134.
22. Yamamoto, T., Togawa, M., Shimada, S., Sangu, N., Shimojima, K., and Okamoto, N. (2014). Narrowing of the responsible region for severe developmental delay and autistic behaviors in WAGR syndrome down to 1.6cMb including PAX6, WT1, and PRRG4. Am. J. Med. Genet. A. *164A*, 634–638.
23. Lehnhardt, A., Karnatz, C., Ahlenstiel-Grunow, T., Benz, K., Benz, M.R., Budde, K., Büscher, A.K., Fehr, T., Feldkötter, M., Graf, N., et al. (2015). Clinical and molecular characterization of patients with heterozygous mutations in wilms tumor suppressor gene 1. Clin. J. Am. Soc. Nephrol. *10*, 825–831.
24. Cai, J., Goodman, B.K., Patel, A.S., Mulliken, J.B., Van Maldergem, L., Hoganson, G.E., Paznekas, W.A., Ben-Neriah, Z., Sheffer, R., Cunningham, M.L., et al. (2003). Increased risk for developmental delay in Saethre-Chotzen syndrome is associated with TWIST deletions: an improved strategy for TWIST mutation screening. Hum. Genet. *114*, 68–76.
25. Gordon, C.T., Tan, T.Y., Benko, S., Fitzpatrick, D., Lyonnet, S., and Farlie, P.G. (2009). Long-range regulation at the SOX9 locus in development and disease. J. Med. Genet. *46*, 649–656.
26. Fernandez, B.A., Siegel-Bartelt, J., Herbrick, J.A., Teshima, I., and Scherer, S.W. (2005). Holoprosencephaly and cleidocranial dysplasia in a patient due to two position-effect mutations: case report and review of the literature. Clin. Genet. *68*, 349–359.
27. de Kok, Y.J., Vossenaar, E.R., Cremers, C.W., Dahl, N., Laporte, J., Hu, L.J., Lacombe, D., Fischel-Ghodsian, N., Friedman, R.A., Parnes, L.S., et al. (1996). Identification of a hot spot for microdeletions in patients with X-linked deafness type 3 (DFN3) 900 kb proximal to the DFN3 gene POU3F4. Hum. Mol. Genet. *5*, 1229–1235.
28. Benko, S., Fantes, J.A., Amiel, J., Kleinjan, D.J., Thomas, S., Ramsay, J., Jamshidi, N., Essafi, A., Heaney, S., Gordon, C.T., et al. (2009). Highly conserved non-coding elements on either side of SOX9 associated with Pierre Robin sequence. Nat. Genet. *41*, 359–364.
29. Amarillo, I.E., Dipple, K.M., and Quintero-Rivera, F. (2013). Familial microdeletion of 17q24.3 upstream of SOX9 is associated with isolated Pierre Robin sequence due to position effect. Am. J. Med. Genet. A. *161A*, 1167–1172.
30. Talkowski, M.E., Ordulu, Z., Pillalamarri, V., Benson, C.B., Blumenthal, I., Connolly, S., Hanscom, C., Hussain, N., Pereira, S., Picker, J., et al. (2012). Clinical diagnosis by whole-genome sequencing of a prenatal sample. N. Engl. J. Med. *367*, 2226–2232.
31. Macera, M.J., Sobrino, A., Levy, B., Jobanputra, V., Aggarwal, V., Mills, A., Esteves, C., Hanscom, C., Pereira, S., Pillalamarri, V., et al. (2015). Prenatal diagnosis of chromothripsis, with nine breaks characterized by karyotyping, FISH, microarray and whole-genome sequencing. Prenat. Diagn. *35*, 299–301.
32. Mills, R.E., Walter, K., Stewart, C., Handsaker, R.E., Chen, K., Alkan, C., Abyzov, A., Yoon, S.C., Ye, K., Cheetham, R.K., et al.;

1000 Genomes Project (2011). Mapping copy number variation by population-scale genome sequencing. Nature *470*, 59–65.
33. Sudmant, P.H., Rausch, T., Gardner, E.J., Handsaker, R.E., Abyzov, A., Huddleston, J., Zhang, Y., Ye, K., Jun, G., Hsi-Yang Fritz, M., et al.; 1000 Genomes Project Consortium (2015). An integrated map of structural variation in 2,504 human genomes. Nature *526*, 75–81.
34. Brand, H., Collins, R.L., Hanscom, C., Rosenfeld, J.A., Pillalamarri, V., Stone, M.R., Kelley, F., Mason, T., Margolin, L., Eggert, S., et al. (2015). Paired-Duplication Signatures Mark Cryptic Inversions and Other Complex Structural Variation. Am. J. Hum. Genet. *97*, 170–176.
35. Brand, H., Pillalamarri, V., Collins, R.L., Eggert, S., O'Dushlaine, C., Braaten, E.B., Stone, M.R., Chambert, K., Doty, N.D., Hanscom, C., et al. (2014). Cryptic and complex chromosomal aberrations in early-onset neuropsychiatric disorders. Am. J. Hum. Genet. *95*, 454–461.
36. Huang, N., Lee, I., Marcotte, E.M., and Hurles, M.E. (2010). Characterising and predicting haploinsufficiency in the human genome. PLoS Genet. *6*, e1001154.
37. Amberger, J.S., Bocchini, C.A., Schiettecatte, F., Scott, A.F., and Hamosh, A. (2015). OMIM.org: Online Mendelian Inheritance in Man (OMIM®), an online catalog of human genes and genetic disorders. Nucleic Acids Res. *43*, D789–D798.
38. Firth, H.V., Richards, S.M., Bevan, A.P., Clayton, S., Corpas, M., Rajan, D., Van Vooren, S., Moreau, Y., Pettett, R.M., and Carter, N.P. (2009). DECIPHER: Database of Chromosomal Imbalance and Phenotype in Humans Using Ensembl Resources. Am. J. Hum. Genet. *84*, 524–533.
39. Bragin, E., Chatzimichali, E.A., Wright, C.F., Hurles, M.E., Firth, H.V., Bevan, A.P., and Swaminathan, G.J. (2014). DECIPHER: database for the interpretation of phenotype-linked plausibly pathogenic sequence and copy-number variation. Nucleic Acids Res. *42*, D993–D1000.
40. Ordulu, Z., Wong, K.E., Currall, B.B., Ivanov, A.R., Pereira, S., Althari, S., Gusella, J.F., Talkowski, M.E., and Morton, C.C. (2014). Describing sequencing results of structural chromosome rearrangements with a suggested next-generation cytogenetic nomenclature. Am. J. Hum. Genet. *94*, 695–709.
41. Shiratsuchi, T., Nishimori, H., Ichise, H., Nakamura, Y., and Tokino, T. (1997). Cloning and characterization of BAI2 and BAI3, novel genes homologous to brain-specific angiogenesis inhibitor 1 (BAI1). Cytogenet. Cell Genet. *79*, 103–108.
42. Rutsch, F., Gailus, S., Miousse, I.R., Suormala, T., Sagné, C., Toliat, M.R., Nürnberg, G., Wittkampf, T., Buers, I., Sharifi, A., et al. (2009). Identification of a putative lysosomal cobalamin exporter altered in the cblF defect of vitamin B12 metabolism. Nat. Genet. *41*, 234–239.
43. Janssen, N., Bergman, J.E., Swertz, M.A., Tranebjaerg, L., Lodahl, M., Schoots, J., Hofstra, R.M., van Ravenswaaij-Arts, C.M., and Hoefsloot, L.H. (2012). Mutation update on the CHD7 gene involved in CHARGE syndrome. Hum. Mutat. *33*, 1149–1160.
44. Laurén, J., Airaksinen, M.S., Saarma, M., and Timmusk, T. (2003). A novel gene family encoding leucine-rich repeat transmembrane proteins differentially expressed in the nervous system. Genomics *81*, 411–421.
45. Castermans, D., Wilquet, V., Parthoens, E., Huysmans, C., Steyaert, J., Swinnen, L., Fryns, J.P., Van de Ven, W., and Devriendt, K. (2003). The neurobeachin gene is disrupted by a translocation in a patient with idiopathic autism. J. Med. Genet. *40*, 352–356.
46. Wise, A., Tenezaca, L., Fernandez, R.W., Schatoff, E., Flores, J., Ueda, A., Zhong, X., Wu, C.F., Simon, A.F., and Venkatesh, T. (2015). Drosophila mutants of the autism candidate gene neurobeachin (rugose) exhibit neuro-developmental disorders, aberrant synaptic properties, altered locomotion, and impaired adult social behavior and activity patterns. J. Neurogenet. *29*, 135–143.
47. Nuytens, K., Gantois, I., Stijnen, P., Iscru, E., Laeremans, A., Serneels, L., Van Eylen, L., Liebhaber, S.A., Devriendt, K., Balschun, D., et al. (2013). Haploinsufficiency of the autism candidate gene Neurobeachin induces autism-like behaviors and affects cellular and molecular processes of synaptic plasticity in mice. Neurobiol. Dis. *51*, 144–151.
48. Lee, S., Takeda, Y., Kawano, H., Hosoya, H., Nomoto, M., Fujimoto, D., Takahashi, N., and Watanabe, K. (2000). Expression and regulation of a gene encoding neural recognition molecule NB-3 of the contactin/F3 subgroup in mouse brain. Gene *245*, 253–266.
49. Fernandez, T., Morgan, T., Davis, N., Klin, A., Morris, A., Farhi, A., Lifton, R.P., and State, M.W. (2004). Disruption of contactin 4 (CNTN4) results in developmental delay and other features of 3p deletion syndrome. Am. J. Hum. Genet. *74*, 1286–1293.
50. Kohwi-Shigematsu, T., Kohwi, Y., Takahashi, K., Richards, H.W., Ayers, S.D., Han, H.J., and Cai, S. (2012). SATB1-mediated functional packaging of chromatin into loops. Methods *58*, 243–254.
51. Alvarez, J.D., Yasui, D.H., Niida, H., Joh, T., Loh, D.Y., and Kohwi-Shigematsu, T. (2000). The MAR-binding protein SATB1 orchestrates temporal and spatial expression of multiple genes during T-cell development. Genes Dev. *14*, 521–535.
52. Balamotis, M.A., Tamberg, N., Woo, Y.J., Li, J., Davy, B., Kohwi-Shigematsu, T., and Kohwi, Y. (2012). Satb1 ablation alters temporal expression of immediate early genes and reduces dendritic spine density during postnatal brain development. Mol. Cell. Biol. *32*, 333–347.
53. Close, J., Xu, H., De Marco García, N., Batista-Brito, R., Rossignol, E., Rudy, B., and Fishell, G. (2012). Satb1 is an activity-modulated transcription factor required for the terminal differentiation and connectivity of medial ganglionic eminence-derived cortical interneurons. J. Neurosci. *32*, 17690–17705.
54. Le Meur, N., Holder-Espinasse, M., Jaillard, S., Goldenberg, A., Joriot, S., Amati-Bonneau, P., Guichet, A., Barth, M., Charollais, A., Journel, H., et al. (2010). MEF2C haploinsufficiency caused by either microdeletion of the 5q14.3 region or mutation is responsible for severe mental retardation with stereotypic movements, epilepsy and/or cerebral malformations. J. Med. Genet. *47*, 22–29.
55. Barbosa, A.C., Kim, M.S., Ertunc, M., Adachi, M., Nelson, E.D., McAnally, J., Richardson, J.A., Kavalali, E.T., Monteggia, L.M., Bassel-Duby, R., and Olson, E.N. (2008). MEF2C, a transcription factor that facilitates learning and memory by negative regulation of synapse numbers and function. Proc. Natl. Acad. Sci. USA *105*, 9391–9396.
56. Middendorp, S., Paoletti, A., Schiebel, E., and Bornens, M. (1997). Identification of a new mammalian centrin gene, more closely related to Saccharomyces cerevisiae CDC31 gene. Proc. Natl. Acad. Sci. USA *94*, 9141–9146.
57. Arking, D.E., Cutler, D.J., Brune, C.W., Teslovich, T.M., West, K., Ikeda, M., Rea, A., Guy, M., Lin, S., Cook, E.H., and Chakravarti, A. (2008). A common genetic variant in the neurexin

superfamily member CNTNAP2 increases familial risk of autism. Am. J. Hum. Genet. *82*, 160–164.
58. Zweier, C., de Jong, E.K., Zweier, M., Orrico, A., Ousager, L.B., Collins, A.L., Bijlsma, E.K., Oortveld, M.A., Ekici, A.B., Reis, A., et al. (2009). CNTNAP2 and NRXN1 are mutated in autosomal-recessive Pitt-Hopkins-like mental retardation and determine the level of a common synaptic protein in Drosophila. Am. J. Hum. Genet. *85*, 655–666.
59. Yu, Z.K., Gervais, J.L., and Zhang, H. (1998). Human CUL-1 associates with the SKP1/SKP2 complex and regulates p21(CIP1/WAF1) and cyclin D proteins. Proc. Natl. Acad. Sci. USA *95*, 11324–11329.
60. Di Meglio, T., Kratochwil, C.F., Vilain, N., Loche, A., Vitobello, A., Yonehara, K., Hrycaj, S.M., Roska, B., Peters, A.H., Eichmann, A., et al. (2013). Ezh2 orchestrates topographic migration and connectivity of mouse precerebellar neurons. Science *339*, 204–207.
61. Chen, H., Rossier, C., and Antonarakis, S.E. (1996). Cloning of a human homolog of the Drosophila enhancer of zeste gene (EZH2) that maps to chromosome 21q22.2. Genomics *38*, 30–37.
62. Belloni, E., Muenke, M., Roessler, E., Traverso, G., Siegel-Bartelt, J., Frumkin, A., Mitchell, H.F., Donis-Keller, H., Helms, C., Hing, A.V., et al. (1996). Identification of Sonic hedgehog as a candidate gene responsible for holoprosencephaly. Nat. Genet. *14*, 353–356.
63. Anderson, E., Devenney, P.S., Hill, R.E., and Lettice, L.A. (2014). Mapping the Shh long-range regulatory domain. Development *141*, 3934–3943.
64. Choucair, N., Mignon-Ravix, C., Cacciagli, P., Abou Ghoch, J., Fawaz, A., Mégarbané, A., Villard, L., and Chouery, E. (2015). Evidence that homozygous PTPRD gene microdeletion causes trigonocephaly, hearing loss, and intellectual disability. Mol. Cytogenet. *8*, 39.
65. Uetani, N., Kato, K., Ogura, H., Mizuno, K., Kawano, K., Mikoshiba, K., Yakura, H., Asano, M., and Iwakura, Y. (2000). Impaired learning with enhanced hippocampal long-term potentiation in PTPdelta-deficient mice. EMBO J. *19*, 2775–2785.
66. Zweier, C., Peippo, M.M., Hoyer, J., Sousa, S., Bottani, A., Clayton-Smith, J., Reardon, W., Saraiva, J., Cabral, A., Gohring, I., et al. (2007). Haploinsufficiency of TCF4 causes syndromal mental retardation with intermittent hyperventilation (Pitt-Hopkins syndrome). Am. J. Hum. Genet. *80*, 994–1001.
67. Kawabe, H., Sakisaka, T., Yasumi, M., Shingai, T., Izumi, G., Nagano, F., Deguchi-Tawarada, M., Takeuchi, M., Nakanishi, H., and Takai, Y. (2003). A novel rabconnectin-3-binding protein that directly binds a GDP/GTP exchange protein for Rab3A small G protein implicated in Ca(2+)-dependent exocytosis of neurotransmitter. Genes Cells *8*, 537–546.
68. Gao, S., Alarcón, C., Sapkota, G., Rahman, S., Chen, P.Y., Goerner, N., Macias, M.J., Erdjument-Bromage, H., Tempst, P., and Massagué, J. (2009). Ubiquitin ligase Nedd4L targets activated Smad2/3 to limit TGF-beta signaling. Mol. Cell *36*, 457–468.
69. Buj-Bello, A., Biancalana, V., Moutou, C., Laporte, J., and Mandel, J.L. (1999). Identification of novel mutations in the MTM1 gene causing severe and mild forms of X-linked myotubular myopathy. Hum. Mutat. *14*, 320–325.
70. Senderek, J., Müller, J.S., Dusl, M., Strom, T.M., Guergueltcheva, V., Diepolder, I., Laval, S.H., Maxwell, S., Cossins, J., Krause, S., et al. (2011). Hexosamine biosynthetic pathway mutations cause neuromuscular transmission defect. Am. J. Hum. Genet. *88*, 162–172.
71. Begemann, M., Zirn, B., Santen, G., Wirthgen, E., Soellner, L., Büttel, H.M., Schweizer, R., van Workum, W., Binder, G., and Eggermann, T. (2015). Paternally Inherited IGF2 Mutation and Growth Restriction. N. Engl. J. Med. *373*, 349–356.
72. Gicquel, C., Rossignol, S., Cabrol, S., Houang, M., Steunou, V., Barbu, V., Danton, F., Thibaud, N., Le Merrer, M., Burglen, L., et al. (2005). Epimutation of the telomeric imprinting center region on chromosome 11p15 in Silver-Russell syndrome. Nat. Genet. *37*, 1003–1007.
73. Jungbluth, H., Wallgren-Pettersson, C., and Laporte, J. (2008). Centronuclear (myotubular) myopathy. Orphanet J. Rare Dis. *3*, 26.
74. Joseph, M., Pai, G.S., Holden, K.R., and Herman, G. (1995). X-linked myotubular myopathy: clinical observations in ten additional cases. Am. J. Med. Genet. *59*, 168–173.
75. Starr, J., Lamont, M., Iselius, L., Harvey, J., and Heckmatt, J. (1990). A linkage study of a large pedigree with X linked centronuclear myopathy. J. Med. Genet. *27*, 281–283.
76. Jeong, Y., El-Jaick, K., Roessler, E., Muenke, M., and Epstein, D.J. (2006). A functional screen for sonic hedgehog regulatory elements across a 1 Mb interval identifies long-range ventral forebrain enhancers. Development *133*, 761–772.
77. Gordon, C.T., Attanasio, C., Bhatia, S., Benko, S., Ansari, M., Tan, T.Y., Munnich, A., Pennacchio, L.A., Abadie, V., Temple, I.K., et al. (2014). Identification of novel craniofacial regulatory domains located far upstream of SOX9 and disrupted in Pierre Robin sequence. Hum. Mutat. *35*, 1011–1020.
78. Bianchi, D.W., Parker, R.L., Wentworth, J., Madankumar, R., Saffer, C., Das, A.F., Craig, J.A., Chudova, D.I., Devers, P.L., Jones, K.W., et al.; CARE Study Group (2014). DNA sequencing versus standard prenatal aneuploidy screening. N. Engl. J. Med. *370*, 799–808.
79. Norton, M.E., Jacobsson, B., Swamy, G.K., Laurent, L.C., Ranzini, A.C., Brar, H., Tomlinson, M.W., Pereira, L., Spitz, J.L., Hollemon, D., et al. (2015). Cell-free DNA analysis for noninvasive examination of trisomy. N. Engl. J. Med. *372*, 1589–1597.
80. Wapner, R.J., Martin, C.L., Levy, B., Ballif, B.C., Eng, C.M., Zachary, J.M., Savage, M., Platt, L.D., Saltzman, D., Grobman, W.A., et al. (2012). Chromosomal microarray versus karyotyping for prenatal diagnosis. N. Engl. J. Med. *367*, 2175–2184.
81. Arbabi, A., Rampášek, L., and Brudno, M. (2016). Cell-free DNA fragment-size distribution analysis for non-invasive prenatal CNV prediction. Bioinformatics *32*, 1662–1669.
82. Drury, S., Williams, H., Trump, N., Boustred, C., Lench, N., Scott, R.H., and Chitty, L.S.; GOSGene (2015). Exome sequencing for prenatal diagnosis of fetuses with sonographic abnormalities. Prenat. Diagn. *35*, 1010–1017.
83. Pangalos, C., Hagnefelt, B., Lilakos, K., and Konialis, C. (2016). First applications of a targeted exome sequencing approach in fetuses with ultrasound abnormalities reveals an important fraction of cases with associated gene defects. PeerJ *4*, e1955.
84. Kearney, H.M., Thorland, E.C., Brown, K.K., Quintero-Rivera, F., and South, S.T.; Working Group of the American College of Medical Genetics Laboratory Quality Assurance Committee (2011). American College of Medical Genetics standards and guidelines for interpretation and reporting of postnatal constitutional copy number variants. Genet. Med. *13*, 680–685.